JOURNAL OF GEOPHYSICAL RESEARCH, VOL. 104, NO. C7, PAGES 15,621–15,634, JULY 15, 1999

Simulations of temperature and turbulence structure of the oceanic boundary layer with the improved near-surface process

Yign Noh and Hyoung Jin Kim

Department of Atmospheric Sciences, Yonsei University, Seoul, Korea

Abstract. An improved model for the oceanic boundary layer is presented in view of the recent observation of the microstructure of the upper ocean including the high dissipation rate near the sea surface. In the new model the surface boundary conditions for both the turbulent kinetic energy flux and the roughness length scale are modified. The parameterization of stratification effects on turbulence is improved, and the convective process is reformulated on the basis of the observation of uniform temperature and velocity profiles within the convective mixed layer. Evolutions of the profiles of both the dissipation rate and temperature of the observation data Patches Experiment as well as the time series of the sea surface temperature over the observation days, are successfully simulated during a diurnal cycle for the first time. It is also shown that the model reproduces various important features of the oceanic boundary layer, for example, the formation of a diurnal thermocline, the profiles of buoyancy flux, and the magnitudes of the buoyancy gradients both within the mixed layer and at the diurnal thermocline. Performance of the model is compared with that of the widely used Mellor-Yamada model.

1. Introduction

Recent measurements of the microstructure of the oceanic boundary layer from various field experiments have revealed that the dynamic process of the oceanic boundary layer is fundamentally different from that of the atmospheric boundary layer [*Shay and Gregg*, 1986; *Agrawal et al.*, 1992; *Anis and Moum*, 1992; *Osborn et al.*, 1992; *Thorpe*, 1992; *Brainerd and Gregg*, 1993a; *Drennan et al.*, 1996; *Toba and Kawamura*, 1996; *Terray et al.*, 1996]. In particular, the observed dissipation rate of turbulence ε near the sea surface is found to be ~2 orders larger than that expected from the wall boundary layer, thus suggesting an equivalently high level of turbulent kinetic energy (TKE). This remarkable enhancement of TKE near the sea surface is attributed to wave breaking and possibly other processes such as wave turbulence interaction and Langmuir circulation, which are unique to the oceanic boundary layer bounded by the free surface [*Kitaigorodskii and Miropolskii*, 1968; *Benilov*, 1973; *Phillips*, 1985; *Kitaigordskii and Lumley*, 1983; *Melville*, 1994; *Anis and Moum*, 1995]. This situation is fundamentally different from the atmospheric boundary layer, which follows the conventional wall boundary layer theory with the logarithmic velocity profile.

A high level of TKE near the sea surface also makes the downward flux of TKE important in the energy budget of the oceanic boundary layer, rendering the contribution from shear production relatively unimportant. Hence, in the upper part of the oceanic boundary layer the balance is made between TKE flux and dissipation, and it leads to the relation for the variation of ε with depth z as $\varepsilon \sim z^{-n}$ with $n \sim 3.0$–4.6. This is contrary to the case of the wall boundary layer in which the relation with $n = 1$ is expected from the balance between shear production and dissipation. It was also observed by *Thorpe* [1992] that the eddy diffusivity remains constant with depth near the sea surface, contrary to the wall boundary layer in which it increases with depth linearly. The situation is analogous to the shear-free turbulence generated by grid oscillation [*Thompson and Turner*, 1975; *Hopfinger and Toly*, 1976], so it suggests that the model for the oscillating grid-generated turbulence [*Noh and Fernando*, 1991; *Craig and Banner*, 1994] can be applied to the oceanic boundary layer. In particular, *Craig and Banner* [1994] suggested a profile of dissipation rate as $\varepsilon \sim z^{-3/4}$ near the sea surface from the model based on the grid-generated turbulence.

The significant difference between the oceanic and atmospheric boundary layer is also evident when the surface heat flux is stabilizing. In the atmospheric boundary layer a strong but continuous temperature gradient appears near the surface during the nighttime. On the other hand, in the oceanic boundary layer a diurnal thermocline is formed at a certain depth during the daytime, and the well-mixed surface layer is usually maintained above the diurnal thermocline, unless the wind is very weak. It was demonstrated by *Noh* [1996] that this significant discrepancy is again attributed to whether the dominant source of turbulence is TKE flux or shear production and that the TKE flux from the sea surface plays a critical role for the formation of a diurnal thermocline. Meanwhile, the large eddy simulation of the oceanic boundary layer by *Skyllingstad and Denbo* [1995] also showed that extremely underestimated TKE appears near the surface during the stabilizing heat flux as long as the wall boundary layer is applied, and they introduced the wave current interaction in order to resolve the problem.

All these evidences from the near-surface process in the oceanic boundary layer, both from observations and numerical simulations, strongly suggest that the model and boundary conditions for the oceanic boundary layer must be fundamen-

Paper number 1999JC900068.
0148-0227/99/1999JC900068$09.00

tally different from those for the atmospheric boundary layer. Nevertheless, most oceanic boundary layer models based on turbulence closure have been developed so far in a similar way to atmospheric boundary layer models, while the physical processes unique to the oceanic boundary layer have been disregarded [*Mellor and Durbin*, 1975; *Klein and Coantic*, 1981; *Andre and Lacarrere*, 1985; *Kantha and Clayson*, 1994; *Large et al.*, 1994]. It is thus not surprising that all the models tend to show too strong a shear and a temperature gradient within the mixed layer, which contradicts the observed uniform profiles of temperature and velocity. This shortcoming of the existing models, caused by neglecting the physical processes unique to the oceanic boundary layer, is also pointed out by *Cane* [1993] and *Garrett* [1996].

On the other hand, the verifications of most oceanic boundary layer models so far have been limited to the comparisons of the time series of the sea surface temperature (SST) or of the mixed layer depths (MLD). They allow the possibility of reproducing these one-dimensional data from a physically unjustifiable model by adjusting various empirical constants. In order to be verified as physically correct the model must be able to predict correctly the evolutions of the vertical profiles of all physical quantities including temperature, salinity, velocity, and dissipation rate as well as SST and MLD.

Therefore, in this study, vertical profiles of the temperature and dissipation rate in the oceanic boundary layer are simulated using a model that is developed on the basis of the recent observations of the near-surface processes. First, simulations are carried out under ideal cases such as heating, cooling, and wind mixing, and the results are examined to determine whether they satisfy the observed general characteristics of the oceanic boundary layer. The simulation is then performed for the real observation data of the Patches Experiment (PATCHEX), where the microstructure profiles of the temperature, salinity, velocity, and the dissipation rate of TKE were measured up to 300 m using the advanced microstructure profiler (AMP). These profiles were taken at 34°N, 127°W, 800 km west of Point Conception during a period of 11 days in October 1986 when winds were generally light [*Lombardo and Gregg*, 1989; *Brainerd and Gregg*, 1993a, b, 1995]. Discussions are made on the basis of the comparisons with the observation and the simulation results from the widely used Mellor-Yamada model [*Mellor and Yamada*, 1982].

2. Model

Equations for the horizontal mean velocity U, the mean buoyancy B, and the mean TKE, E, in the oceanic boundary layer can be written as [see, e.g., *Phillips*, 1977]

$$\frac{\partial U}{\partial t} = -\frac{\partial}{\partial z}\overline{uw} + f \times U \tag{1}$$

$$\frac{\partial B}{\partial t} = -\frac{\partial}{\partial z}\overline{bw} - \frac{\partial R}{\partial z} \tag{2}$$

$$\frac{\partial E}{\partial t} = -\frac{\partial}{\partial z}\overline{w\left(\frac{p}{\rho_0} + uu + w^2\right)} - \overline{uw}\frac{\partial U}{\partial z} - \overline{bw} - \varepsilon \tag{3}$$

if horizontal homogeneity is assumed. Here u and w are the horizontal and vertical components of fluctuating velocity, b is the fluctuating buoyancy ($= -g\Delta\rho/\rho_0$), p is the fluctuation of pressure, ε is the dissipation rate of TKE, f is the Coriolis parameter, and R is the penetration of solar radiation. The vertical coordinate z is directed downward from the sea surface. The terms on the right-hand side of (3) represent the flux of TKE, the production by mean velocity shear, the decay or production by buoyancy flux, and the turbulence dissipation, respectively. The prescription for the penetration of solar radiation follows that by *Paulson and Simpson* [1977] as suggested by *Brainerd and Gregg* [1993b].

Introducing the eddy diffusivity and eddy viscosity, (1)–(3) can be rewritten as

$$\frac{\partial U}{\partial t} = \frac{\partial}{\partial z}\left(K\frac{\partial U}{\partial z}\right) + fU \tag{4}$$

$$\frac{\partial B}{\partial t} = \frac{\partial}{\partial z}\left(K_B\frac{\partial B}{\partial z}\right) - \frac{\partial R}{\partial z} \tag{5}$$

$$\frac{\partial E}{\partial t} = \frac{\partial}{\partial z}\left(K_E\frac{\partial E}{\partial z}\right) + K\frac{\partial U}{\partial z}\frac{\partial U}{\partial z} + K_B\frac{\partial B}{\partial z} - \varepsilon \tag{6}$$

Here K is the eddy viscosity, and K_B and K_E are the eddy diffusivities for B and E, respectively. They can be modeled as

$$K = Sql \tag{7}$$

$$K_B = S_B ql \tag{8}$$

$$K_E = S_E ql \tag{9}$$

where q is the rms velocity of turbulence [$= (2E)^{1/2}$] and l is the length scale of turbulence. The dissipation rate can be modeled as

$$\varepsilon = Cq^3 l^{-1} \tag{10}$$

As long as there is no stratification, the constants are taken as $S = 0.39\ (= S_0)$, $Pr\ (= S/S_B) = 0.8$, $\sigma(= S/S_E) = 1.95$, and $C = 0.06\ (= C_0)$, which are the same as in the *Mellor-Yamada* [1982] model; here subscript 0 represents the values of the empirical coefficients in the absence of stratification. Similar values have also been used in other models; for example, $S_0 = 0.33$, $Pr = 0.8$, $\sigma = 1.37$, and $C_0 = 0.04$ by *Davies and Jones* [1988].

The boundary conditions at the sea surface ($z = 0$) are given by

$$K\frac{\partial U}{\partial z} = \tau/\rho_0 \tag{11}$$

$$K_B\frac{\partial B}{\partial z} = Q_0 \tag{12}$$

$$K_E\frac{\partial E}{\partial z} = mu_*^3 \tag{13}$$

and no net fluxes of TKE, buoyancy, and momentum are assumed at the bottom. Here τ are the wind stresses, u_* is the frictional velocity defined by ${u_*}^2 = \tau/\rho_0$, Q_0 is the buoyancy flux at the sea surface, and m is the empirical constant determining the TKE flux at the sea surface.

The typical boundary conditions for the TKE flux and the roughness length scale in the atmospheric boundary layer are given by $m = 0$ and $z_0 = 0$ m, and the same boundary conditions have been applied in most oceanic boundary layer models so far [*Mellor and Durbin*, 1975; *Klein and Coantic*, 1981; *Andre and Lacarrere*, 1985; *Kantha and Clayson*, 1994]. These boundary conditions are based on the wall boundary

layer, which is found to be inapplicable to the oceanic boundary layer, as elucidated earlier. These boundary conditions are also inconsistent with the observation that shows the maximum eddy diffusivity near the sea surface [*Thorpe*, 1992; *Yu and O'Brien*, 1991]. In particular, *Noh* [1996] found that it is not possible either to form a diurnal or seasonal thermocline or to maintain a well-mixed layer near the surface under stabilizing buoyancy flux as long as these boundary conditions are used and thus argued that much larger values are required for both m and z_0 in the oceanic boundary layer model.

Recently, *Craig and Banner* [1994] suggested the values for m and z_0 as $m = 100$ and $z_0 = 1$ m on the basis of the comparison with the measurements of the dissipation rate by *Agrawal et al.* [1992], *Anis and Moum* [1992], and *Osborn et al.* [1992]. So, we will assign the values for m and z_0 following *Craig and Banner* [1994]. The appropriateness of these values will be reexamined in the present study, however, from the comparison with the observation data.

The length scale l is given by

$$l = \frac{\kappa(z + z_0)}{1 + \kappa(z + z_0)/h} \tag{14}$$

where z_0 is the roughness length scale, κ is the von Karman constant, and h is the mixed layer depth. The mixed layer depth is defined by the depth of the maximum buoyancy gradient, which also coincides with the depth where the TKE flux from the sea surface disappears. Note that the use of the *Blackadar* [1962] length scale, which is widely used in other models [*Mellor and Durbin*, 1975; *Klein and Coantic*, 1981; *Andre and Lacarrere*, 1985; *Kantha and Clayson*, 1994], becomes inappropriate in the presence of a very high TKE level near the sea surface.

The proportional constants S, S_B, S_E, and C are affected by the density stratification of the fluid. It has been suggested that the growth of the vertical length scale of turbulence is limited by the buoyancy length scale l_b ($= q/N$, where N is the Brunt-Väisälä frequency, i.e., $N^2 = -\partial B/\partial z$) in stably stratified fluids [*Csanady*, 1964; *Britter et al.*, 1983; *Wyngaard*, 1985]. The eddy viscosity is then estimated by

$$K \sim q l_b \sim q l \, \mathrm{Ri}_t^{-1/2} \tag{15}$$

where

$$\mathrm{Ri}_t = (Nl/q)^2 \tag{16}$$

is the Richardson number for turbulent eddies. On the basis of the estimation (15) at large Ri_t, S can be represented by

$$S/S_0 = (1 + \alpha \, \mathrm{Ri}_t)^{-1/2} \tag{17}$$

with an empirical coefficient α. The value of α is determined from the comparison of the model results with the observation data in the present study as $\alpha \cong 120$. Similarly, the effect of stratification on C is given by

$$C/C_0 = (1 + \alpha \, \mathrm{Ri}_t)^{1/2} \tag{18}$$

It is also assumed that Pr and σ are independent of Ri_t, as it is known that the effects of stratification on them are very weak [*Mellor and Yamada*, 1982]. The basic presumption made in (17) and (18) is that what determines the eddy diffusivity is the kinetic energy of the eddies overcoming stratification regardless of whether the turbulence is produced by velocity shear, buoyancy, or TKE fluxes.

In contrast to this, in the Mellor-Yamada model [*Mellor and Yamada*, 1982] the parameterization of the effects of stratification on S is based on the assumption that the shear production is a dominant term for turbulence production. In their model of level 2, for example, it is given by

$$S = a_1 \frac{1 - a_2 \, \mathrm{Ri}_f}{1 - a_3 \, \mathrm{Ri}_f} \tag{19}$$

where a_1, a_2, and a_3 are constants and Ri_f is the flux Richardson number defined by

$$\mathrm{Ri}_f = -\frac{S_B}{S} \frac{\partial B/\partial z}{[(\partial U/\partial z)^2 + (\partial V/\partial z)^2]} \tag{20}$$

It is evident that Ri_f is not an appropriate parameter for the turbulence in the oceanic boundary layer dominated by the TKE flux, and in particular, it becomes infinite in shear-free turbulence. Moreover, the remarkable difference in the parameterizations by (17) and (19) is that S becomes zero in (19) if stratification increases to a certain level ($\mathrm{Ri}_f = a_2^{-1} = 0.19$), whereas S given by (17) gradually decreases with stratification but maintains a positive value.

Note that turbulence is composed of eddies of many different sizes and that the eddies smaller than l_b are not strongly affected by stratification and so still contribute to turbulent mixing [*Hopfinger*, 1987; *Stillinger et al.*, 1983]. This suggests that the eddy diffusivity may not go to zero, even if the flux Richardson number based on the mean velocity shear exceeds a critical value.

The representation of convection has still remained as a difficult part in the modeling of the planetary boundary layer since the application of eddy diffusivity does not work very well, often causing unrealistic results such as the countergradient buoyancy transfer [*Stull*, 1988; *Wyngaard*, 1985]. To cope with this problem, various attempts have been made for the oceanic boundary layer model, and highly complex models based on the second-moment closure scheme, similar to the atmospheric boundary layer model, have been developed that involve a large number of empirical constants and equations [*Kantha and Clayson*, 1994; *Klein and Coantic*, 1981; *Andre and Lacarrere*, 1985]. Nevertheless, such models are based on the same assumptions as are used for the atmospheric boundary layer, which may not be valid any more in the ocean. Moreover, the important three-dimensional phenomena in the oceanic boundary layer such as Langmuir circulation are still neglected.

On the other hand, the recent measurement by *Anis and Moum* [1994] confirmed that during convection the vertical profiles of velocity and temperature of the oceanic boundary layer are virtually uniform, which is consistent with the assumption used in bulk models of the oceanic boundary layer [*Kraus and Turner*, 1967; *Niiler and Kraus*, 1977; *Garwood*, 1977; *Price et al.*, 1986; *Gaspar*, 1988]. Therefore, to represent convection in this model, uniform mixing is forced for both buoyancy and velocity whenever the unstable stratification occurs, i.e., the buoyancy gradient becomes positive $\partial B/\partial z > 0$, similarly to the model by *Price et al.* [1986]. In this way the fluxes of buoyancy and momentum are represented separately above and below the mixed layer depth, i.e., if $z < h$,

$$-\overline{bw} = Q_0 - (Q_0 - Q_h)\frac{z}{h} \tag{21}$$

$$-\overline{uw} = \frac{1}{\rho_0}\left[\tau - (\tau - \tau_h)\frac{z}{h}\right] \tag{22}$$

as used in bulk models [*Niiler and Kraus*, 1977], but if $z > h$,

$$-\overline{bw} = K_B \frac{\partial B}{\partial z} \tag{23}$$

$$-\overline{uw} = K \frac{\partial U}{\partial z} \tag{24}$$

in the same manner as in the stable boundary layer. Here h is the depth of the mixed layer during convection, and Q_h and τ_h are the values of buoyancy and momentum fluxes at the base of the mixed layer, which are calculated by (23) and (24).

Remarkably, it has been observed, however, that the vertical distribution of the dissipation rate, which is determined basically by the magnitude of TKE, still maintains a strong gradient near the surface regardless of its stability condition, although velocity and temperature are uniformly mixed within the convective mixed layer [*Shay and Gregg*, 1986; *Anis and Moum*, 1992]. Note that TKE decays with time because of dissipation while being transferred downward unlike momentum and heat. Therefore, in order to be mixed effectively over the whole mixed layer by convective eddies the decaying timescale of TKE must be much larger than the overturning timescale of convective eddies. On the other hand, the flux of TKE is important in the oceanic boundary layer only because of the presence of small-scale eddies of high intensity near the sea surface presumably produced by wave breaking. So, it suffices to consider the convective transport of TKE of these small-scale eddies near the sea surface. The length scale of these eddies (l_s), which is comparable to the dominant wave length of surface waves [*Melville*, 1994; *Phillips*, 1985], is much smaller in general than the length scale of convective eddies (l_c), which is comparable to the mixed layer depth. Meanwhile, the velocity scale of dominant eddies (q_s) is much larger than that of convective eddies (q_c) as evidenced by *Shay and Gregg* [1986] and *Anis and Moum* [1994]. As a result, the decaying timescale of the dominant eddies is much smaller than the overturning timescale of larger convective eddies, i.e.,

$$l_s/q_s \ll l_c/q_c \tag{25}$$

Therefore, large convective eddies, which are responsible for the transport of momentum and heat over the whole depth of the convective mixed layer, cannot transport TKE of the small-scale eddies effectively. On the basis of this argument it is assumed in the present model that the TKE flux and dissipation rate are not affected by convective eddies.

The basic principle for the development of the present model is to formulate a simple model that is able to reproduce the evolutions of the vertical structures of the oceanic boundary layer, especially the recently observed microstructure in the upper ocean. At this point it does not appear to make much sense to develop a highly complicated model composed of numerous equations and empirical constants, for the fundamental nature of the upper ocean process itself is still far from being clearly understood. Besides, we prefer to develop a simple model that can be embedded into the ocean general circulation model without causing an unnecessary burden to computation. We also try to avoid the introduction of empirical constants as much as possible. In the present model the roughness length scale z_0, the coefficient determining the TKE flux at the surface m, and the coefficient representing the effects of stratification on turbulence α are the only empirical parameters except for the coefficients for the eddy viscosity, eddy diffusivity, and the dissipation rate in (7)–(10), which were introduced by *Mellor and Yamada* [1982].

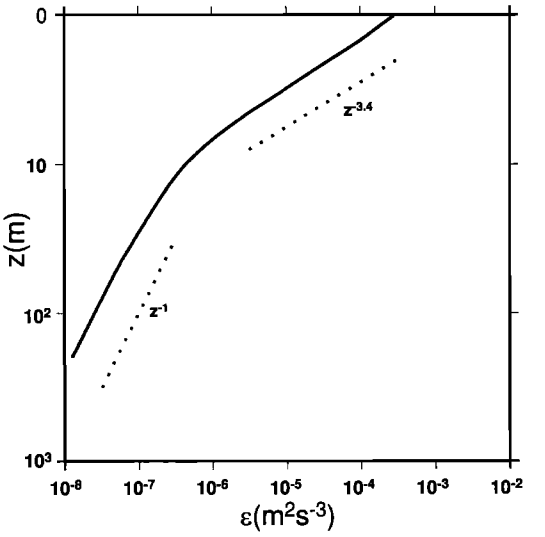

Figure 1. The vertical profile of dissipation rate in the homogeneous oceanic boundary layer ($u_* = 0.01$ m s^{-1}).

3. General Characteristics of the Model

Before simulating the observed data, which are usually influenced by complicated boundary conditions and various kinds of uncertainty, it is important to examine whether the general characteristics of the present model are consistent with those known for the oceanic boundary layer. Therefore simulations were first carried out for the ideal cases such as the homogeneous boundary layer, the formation of a diurnal thermocline under heating, convective mixing under cooling, and the deepening of the mixed layer by wind stress.

First, the vertical profile of the dissipation rate of the homogeneous boundary layer under the wind stress ($u_* = 0.01$ m s^{-1}) is shown in Figure 1. The relation $\varepsilon \sim z^{-1}$, corresponding to the wall boundary layer, is observed away from the surface, but the dissipation rate increases sharply as it approaches the sea surface. The transition occurs at a depth of ~10 m, and the upper region will be called the near-surface zone of the high dissipation rate. In the near-surface zone the exponential coefficient n in the relation $\varepsilon \sim z^{-n}$ is slightly smaller than 3.4, the value suggested by *Craig and Banner* [1994] for the case of TKE flux only since both TKE flux and shear production exist here.

Figure 2 shows the evolutions of the vertical distributions of B, ε, and buoyancy flux Q, which were calculated from the model under the constant stabilizing buoyancy flux and wind stress ($Q_0 = 1.0 \times 10^{-6}$ m^2 s^{-3} and $u_* = 0.01$ m s^{-1}). It can be seen clearly from the evolution of buoyancy (Figure 2a) that a diurnal thermocline is formed with time at a certain depth. The depth is found to be determined by the Monin-Obukhov length scale L ($= u_*^3/Q_0$), which represents the depth where the downward propagation of turbulence by TKE flux is limited by stabilizing buoyancy force [*Kitaigorodskii*, 1970; *Kraus*, 1988; *Noh*, 1996]. Weak stratification of $N^2 \sim 10^{-5}$ s^{-2} appears within the mixed layer (Figure 2a). It is consistent with the observations by *Brainerd and Gregg* [1993a] and *Anis and Moum* [1994], in which weak stratification up to

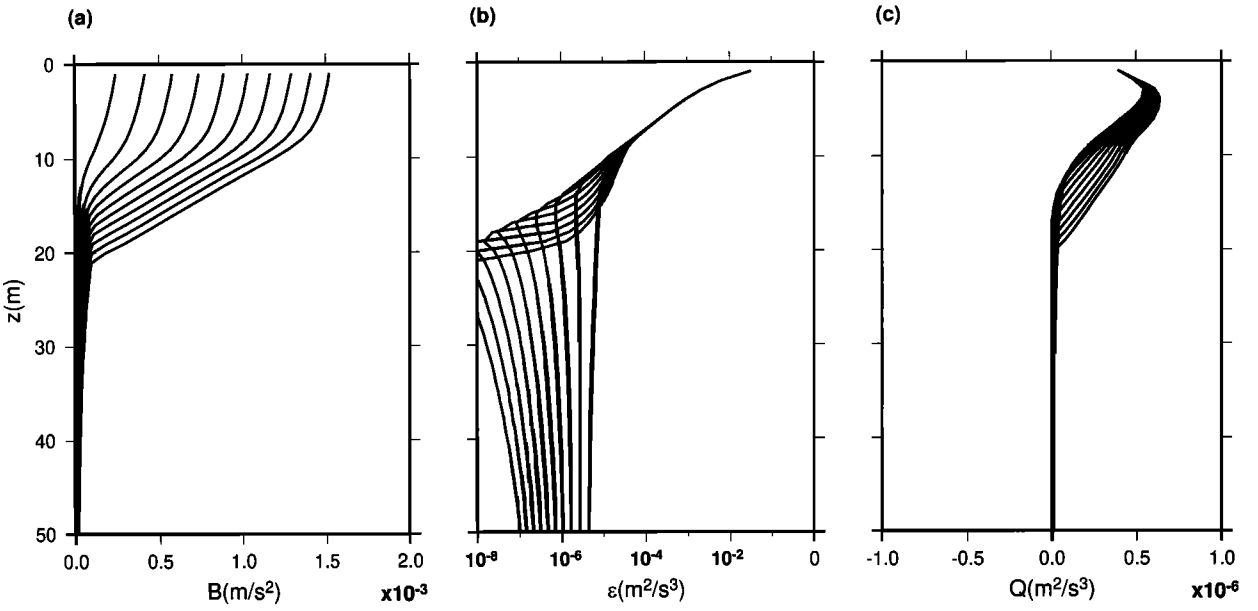

Figure 2. Evolution of the oceanic boundary layer under stabilizing buoyancy flux and wind stress (Q_O = 10^{-6} m^2 s^{-3} and u_* = 0.01 m s $^{-1}$) and no initial stratification (Δt = 2 × 10^3s): (a) buoyancy, (b) dissipation rate, and (c) buoyancy flux.

$N^2 \sim 10^{-5}$ s^{-2} appears within the mixed layer above the diurnal thermocline during heating while it remains virtually uniform during convection. The simulation result that the diurnal thermocline having the stratification of $N^2 \sim 10^{-4}$ s^{-2} increases its thickness gradually with time also agrees well with *Brainerd and Gregg*'s [1993a, b] observation. The thickness of a diurnal thermocline grows with time because heat is transferred downward below the thermocline by radiation penetration and by the turbulence maintained below the thermocline because of shear production [*Brainerd and Gregg*, 1993b; *Noh*, 1996]. The dissipation rate (Figure 2b) decreases continuously below the diurnal thermocline once it is formed because TKE flux cannot be propagated across the diurnal thermocline [*Noh*, 1996]. A high dissipation rate is maintained, however, within the mixed layer.

The convective mixing process is shown in Figure 3, where the calculation was carried out under the constant unstabilizing buoyancy flux ($Q_0 = -1.0 \times 10^{-6}$ m^2 s^{-3}) starting from the initially uniformly stratified layer with $N^2 = 10^{-4}$ s^{-2}. Figure 3a shows the deepening of the uniform convective mixed layer with time. The dissipation rate within the convective mixed layer can be scaled by the surface buoyancy flux Q_0, while its value increases steeply up to 2 orders of magnitude as it approaches the surface (Figure 3b). This agrees with the observation of the dissipation rate during convection [*Shay and Gregg*, 1986; *Lombardo and Gregg*, 1989; *Anis and Moum*, 1994]. It can be also inferred from Figure 2b that the turbulence production is dominated by the TKE flux from the surface up to a depth of ~10 m, then it is dominated by convection. Buoyancy flux (Figure 3c) is found to vary linearly with depth in the mixed layer during cooling as represented by (21). Meanwhile, the buoyancy flux of the opposite direction, caused by entrainment, appears at the bottom of the mixed layer during convection. The amount of buoyancy flux at the bottom of the mixed layer Q_h remains proportional to Q_0 during the deepening; that is, $Q_h = \beta Q_0$ with $\beta \sim 0.1$–0.4, comparable to the atmospheric boundary layer [*Stull*, 1988]. In the ocean it has been observed by *Anis and Moum* [1994] as $\beta \cong 0.13$.

Finally, the wind-deepening experiment was carried out under the constant strong wind stress (u_* = 0.02 m s^{-1}) in the absence of buoyancy flux starting from the initially uniformly stratified layer with $N^2 = 10^{-4}$ s^{-2} (Figure 4). The TKE below the near-surface zone of high dissipation is found to maintain a constant value that can be scaled by u_*^3 (not shown), thus leading to the dissipation rate profiles estimated by u_*^3/z (Figure 4b). It suggests that the shear production is the dominant source of TKE below the near-surface zone. As expected from the fact that the present model allows TKE below the mixed layer, the deepening is found to be more efficient than in the case of the Mellor-Yamada model, which is known to cause insufficient mixing under stratification [*Martin*, 1985; *Rosati and Miyakoda*, 1988].

4. Simulation of PATCHEX Data

Nearly 700 microstructure profiles, taken during PATCHEX with average 2.4 drops per hour, comprise 11 cycles of daytime stratification and nighttime convection in the oceanic boundary layer during a period of generally light winds. Microstructure profiles of temperature, salinity, velocity, and the dissipation rate of TKE were measured up to 300 m together with the corresponding meteorological condition. A more detailed measuring process is described by *Lombardo and Gregg* [1989] and *Brainerd and Gregg* [1993a, b, 1995].

Figures 5 and 6 show the evolutions of the dissipation rate and temperature on typical days (October 16 and 17) with moderate winds and a normal buoyancy flux cycle. Near the surface a region of an elevated dissipation rate and almost uniform temperature persists throughout the daily cycle. The diurnal thermocline starts to form at a depth of ~10 m after the surface buoyancy flux turns positive in the morning. Once the diurnal thermocline is formed, incoming heat energy is

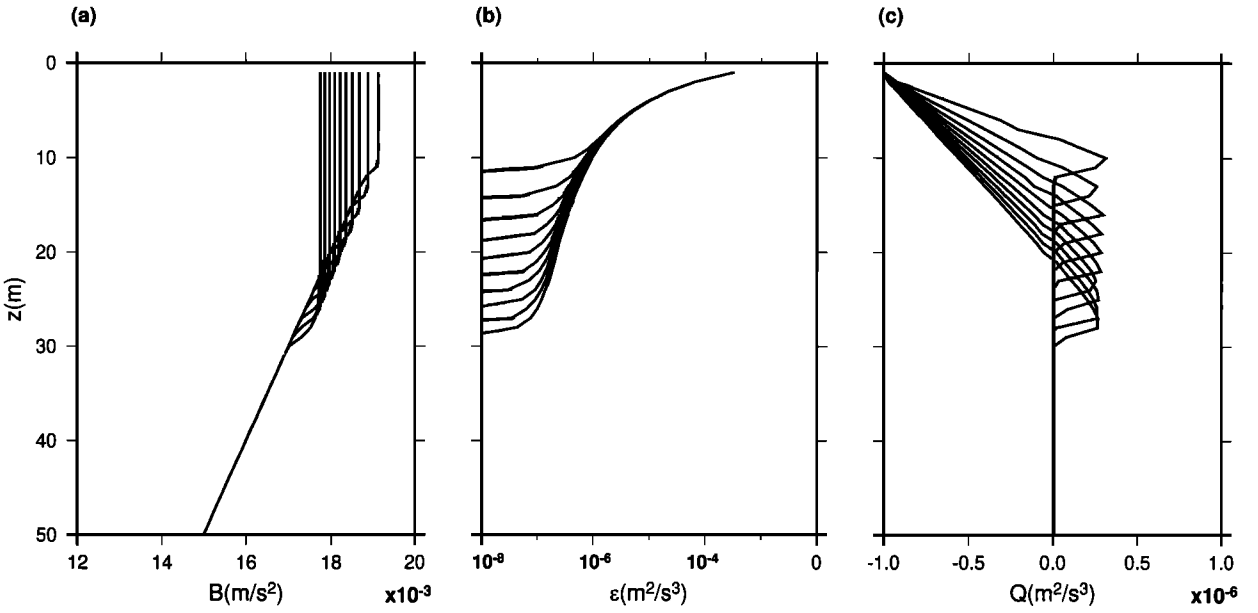

Figure 3. Evolution of the oceanic boundary layer under unstabilizing buoyancy flux and wind stress ($Q_O = -10^{-6}$ m^2 s^{-3} and $u_* = 0.01$ m s^{-1}) and the initial stratification $N^2 = 10^{-4}$ s^{-2} ($\Delta t = 2 \times 10^3$ s): (a) buoyancy, (b) dissipation rate, and (c) buoyancy flux.

mostly accumulated within the mixed layer above it. In the remnant layer below the diurnal thermocline the buoyancy gradient increases and the dissipation rate decreases gradually with time. When the buoyancy flux turns negative in the evening, the diurnal thermocline is driven deeper by convection, reaching the seasonal thermocline of ~50 m deep at night. The increased dissipation rate and virtually uniform temperature appear within the convective mixed layer.

Simulation of the oceanic boundary layer was carried out for the corresponding days using the present model on the basis of the observed wind stress and buoyancy flux, and the results are shown in Figures 7 and 8. The variation of salinity was not considered during the simulation, as it was inferred that the density of seawater was dominated by temperature variation. The seasonal thermocline was also absent, presuming that it did not affect the oceanic boundary layer above. Since we are concerned with only the upper part of the oceanic boundary layer, the difference between temperature and potential temperature was also neglected.

Figures 7 and 8 show the simulated evolutions of ε and T corresponding to the observation data of Figures 5 and 6. Simulation could reproduce well the various aspects of a diur-

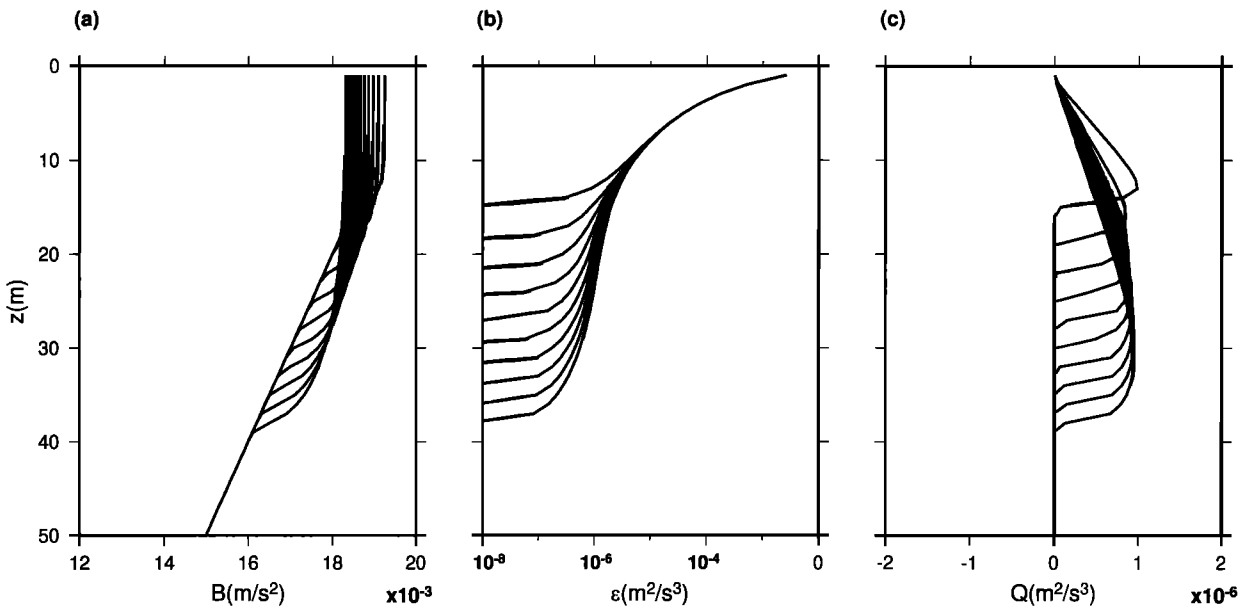

Figure 4. Evolution of the oceanic boundary layer under wind stress only ($u_* = 0.02$ m s^{-1}) and the initial stratification $N^2 = 10^{-4}$ s^{-2} ($\Delta t = 2 \times 10^3$ s): (a) buoyancy, (b) dissipation rate, and (c) buoyancy flux.

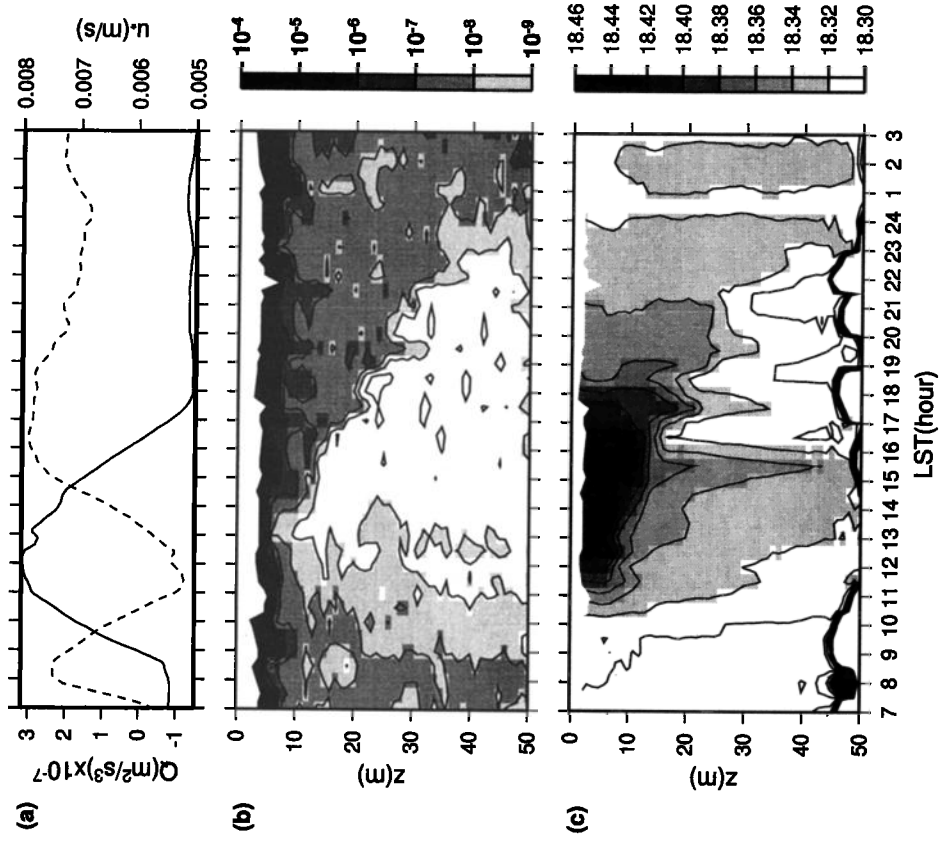

Figure 6. Evolution of the oceanic boundary layer from the observation (October 17): (a) surface buoyancy flux (solid line) and friction velocity (dashed line), (b) dissipation rate ($m^2\ s^{-3}$), and (c) temperature (°C).

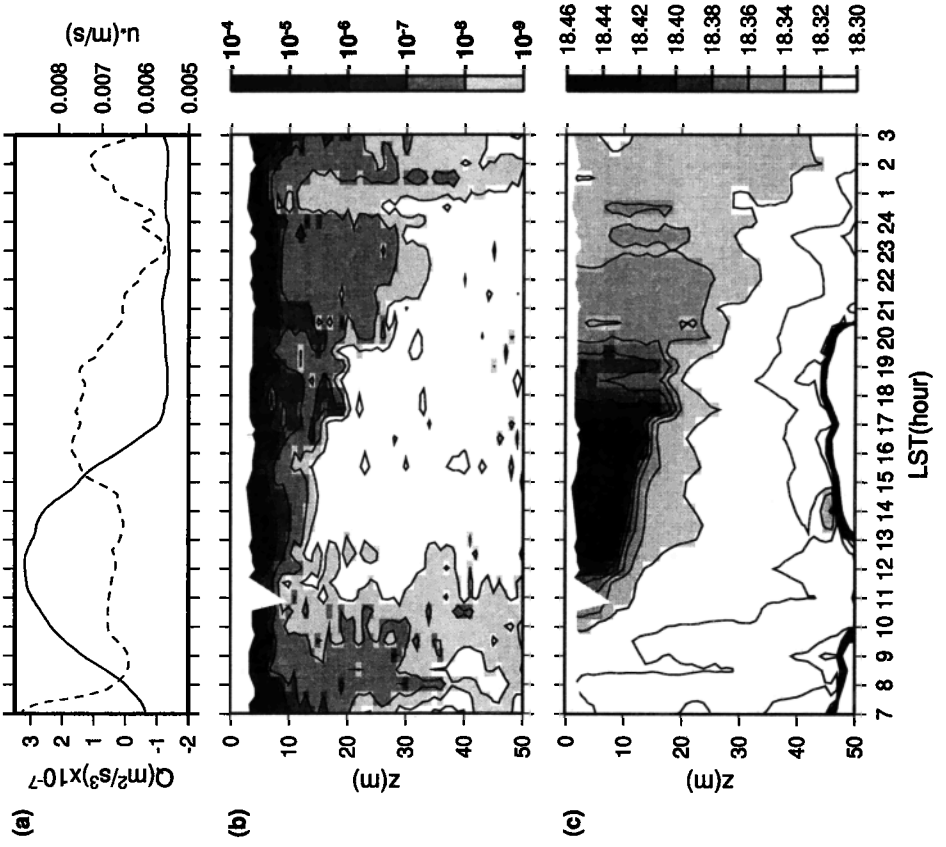

Figure 5. Evolution of the oceanic boundary layer from the observation (October 16): (a) surface buoyancy flux (solid line) and friction velocity (dashed line), (b) dissipation rate ($m^2\ s^{-3}$), and (c) temperature (°C).

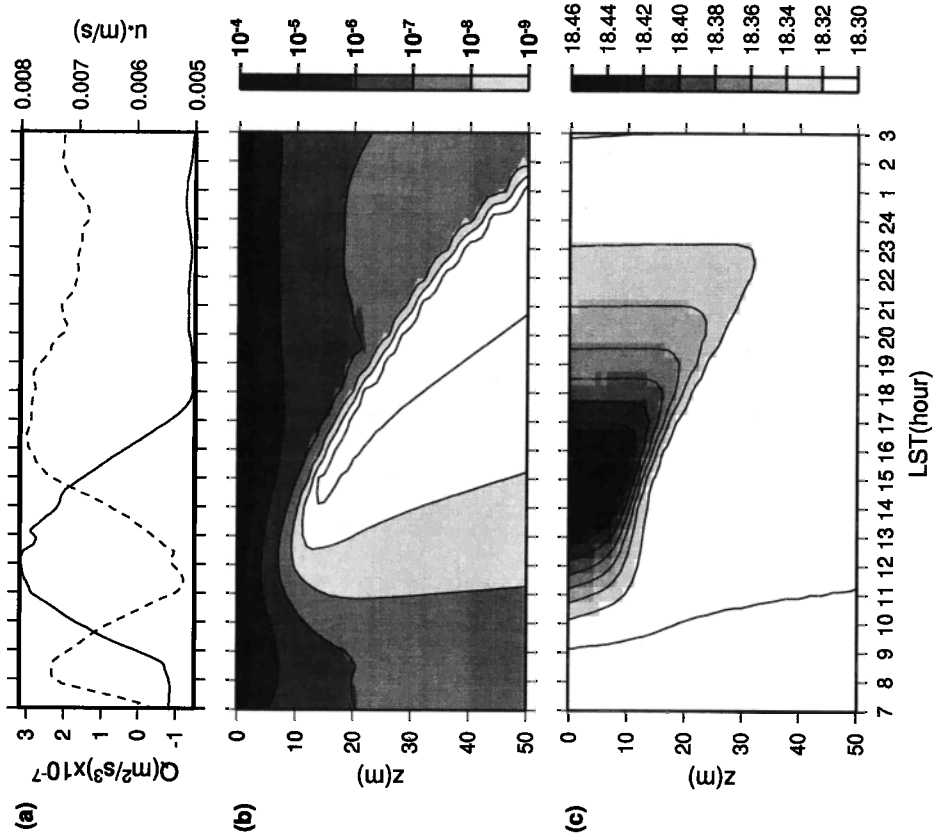

Figure 8. Evaluation of the oceanic boundary layer from the simulation (October 17): (a) surface buoyancy flux (solid line) and friction velocity (dashed line), (b) dissipation rate ($m^2\ s^{-3}$), and (c) temperature (°C).

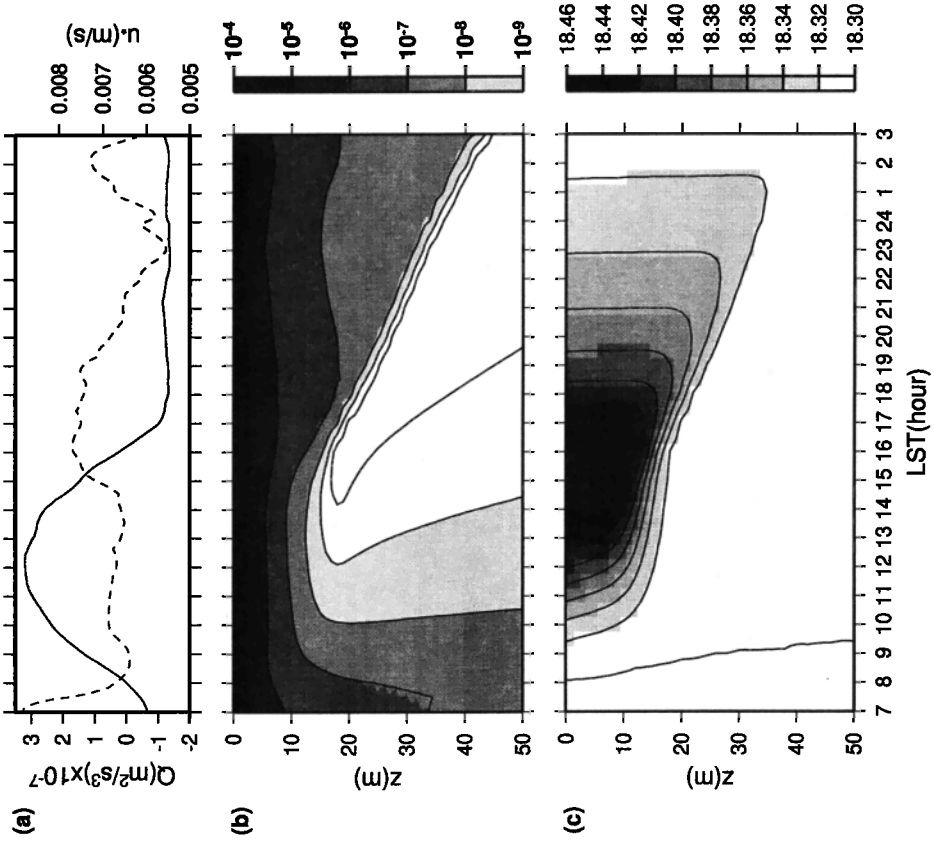

Figure 7. Evolution of the oceanic boundary layer from the simulation (October 16): (a) surface buoyancy flux (solid line) and friction velocity (dashed line), (b) dissipation rate ($m^2\ s^{-3}$), and (c) temperature (°C).

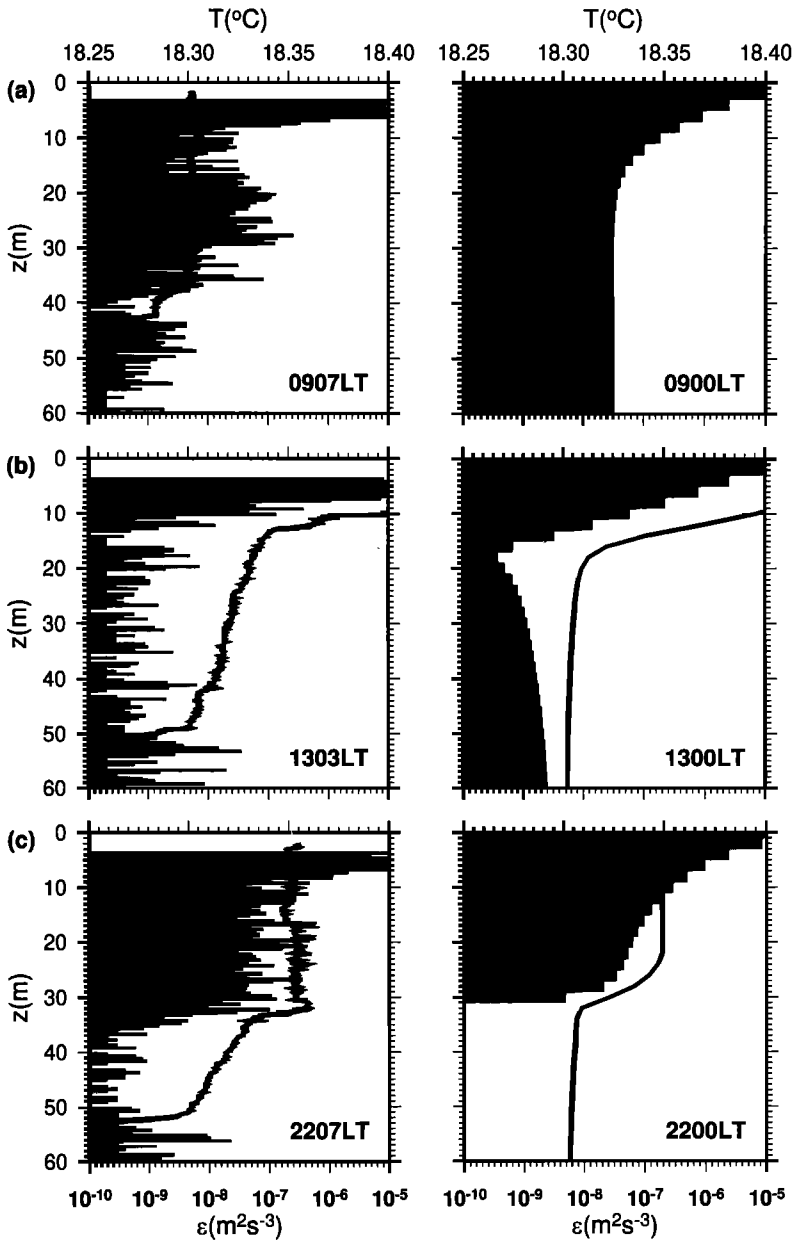

Figure 9. Profiles of dissipation rate and temperature from the observation and the simulation (October 16): (a) neutral boundary layer, (b) stable boundary layer, and (c) convective boundary layer.

nal cycle of the oceanic boundary layer described above, for example, the formation of a diurnal thermocline, convective deepening, and the high dissipation rate near the surface.

On the other hand, it is noticed that the observed temperature below the diurnal thermocline tends to be higher than the simulated one. *Brainerd and Gregg* [1993a, b] suggested that the lateral advection, such as relaxation of horizontal density inhomogeneities into restratification, contributed as much as 40% restratification below the mixed layer, which results in a higher temperature than is expected from the vertical heat transfer only. It should also be mentioned that the modifications in either the radiation penetration or the parameterization of stratification effects on turbulence, i.e., the value of α, could not remove the disagreement as long as the variations of SST and MLD were reasonably reproduced.

For a more detailed comparison the vertical profiles of T and ε, from the observation and the simulation, are presented representing three typical stages of the diurnal cycle of the oceanic boundary layer for the case of October 16 (Figure 9): (1) the neutral boundary layer without buoyancy flux at 0907 LT, (2) the stable boundary layer during the positive buoyancy flux at 1303 LT, and (3) the convective boundary layer during the negative buoyancy flux at 2207 LT. Here the corresponding profiles from the simulation are chosen from those produced at hourly intervals. A good agreement in the neutral boundary layer suggests that the estimations of m and z_0 by *Craig and Banner* [1994] are within reasonable ranges. Temperature below the diurnal thermocline is slightly higher in the observation than in the simulation, as mentioned above (Figure 9b).

A simulation was also carried out using the Mellor-Yamada model of level $2\frac{1}{2}$ [*Mellor and Yamada*, 1982] under the same situation (October 16) for the sake of comparison, and the

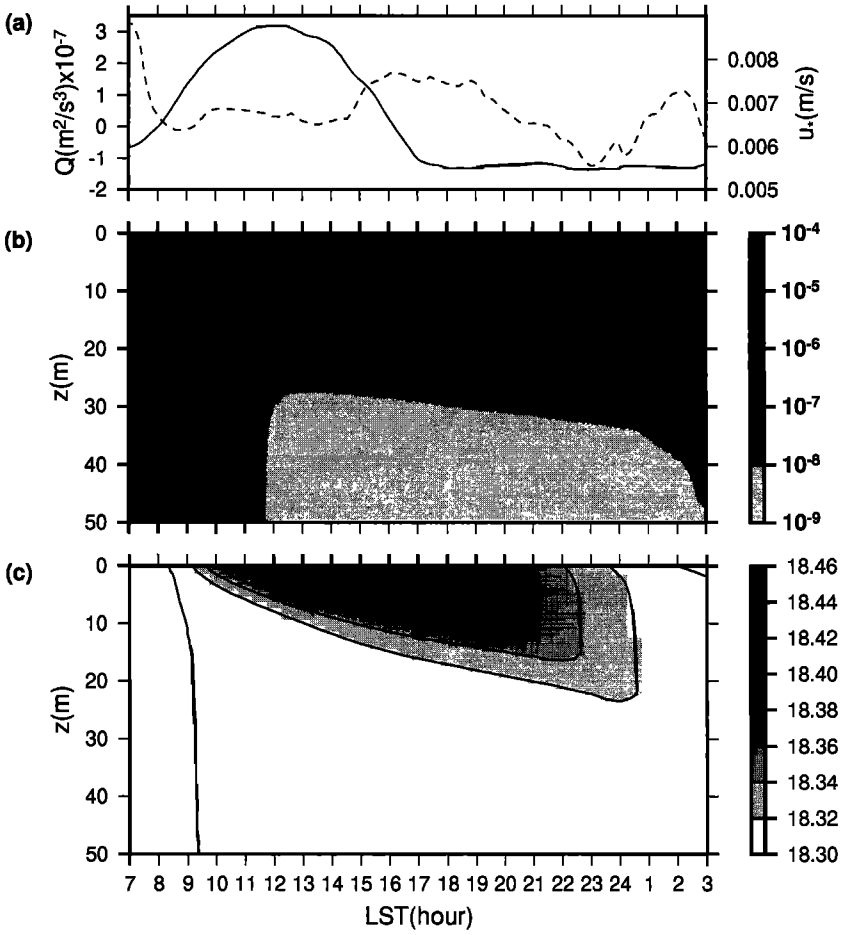

Figure 10. Evolution of the oceanic boundary layer from the simulation (October 16) by the Mellor-Yamada model of level $2\frac{1}{2}$: (a) surface buoyancy flux (solid line) and friction velocity (dashed line), (b) dissipation rate ($m^2\ s^{-3}$), and (c) temperature (°C).

results are shown in Figure 10. Here the boundary conditions for m and z_0 were assigned as $m = 0$ and $z_0 = 0$ m, as are used in the Mellor-Yamada model.

It is evident in Figure 10 that during the daytime a diurnal thermocline is not formed, and heat accumulates near the surface, causing strong stratification, as in the case of the atmospheric boundary layer, thus leading to the serious overestimation of the sea surface temperature. On the other hand, during convection an unrealistically strong inverse buoyancy gradient appears within the mixed layer, and the deepening is significantly slower than the observation. Above all, it is found that the model cannot reproduce the general pattern of the evolutions of the observed dissipation rate profiles, not even qualitatively.

The application of the Mellor-Yamada model with the modified boundary conditions such as $m = 100$ and $z_0 = 1$ m may not make much sense because the model was developed on the basis of the assumption of the negligible effects of TKE flux. The simulation results for other days are also shown in Figures 11 and 12 and compared with the corresponding observations of October 13 and 18 (Figures 13 and 14), which characterize the typical conditions of weak and strong wind stresses, respectively. The results substantiate that good agreements are still observed under quite different conditions. It is also found that the very weak buoyancy flux during the night of October 13 (Figure 13) cannot induce sufficient convective mixing over the whole mixed layer depth.

Finally, the simulation of the variation of SST, which has been the most conventional way of verifying the oceanic boundary layer model, was also carried out over the days of PATCHEX (Figure 15). The days after October 21 are not considered because of the problem in the data [*Brainerd and Gregg*, 1993a]. The comparison with the observation data reveals good agreement between two data except for the nights of October 14 and 15, where a stratified intrusion in the remnant layer prevented a convective deepening process, as mentioned by *Brainerd and Gregg* [1993a]. The result again supports that the choices of empirical constants m, z_0, and α are appropriate.

5. Conclusion and Discussion

In this paper a fairly simple model for the oceanic boundary layer was presented with an aim to resolve the persistent inconsistency between existing turbulence models and observations, especially in view of the recent observation of the microstructure of the upper ocean including the high dissipation rate near the sea surface. The model was able to reproduce successfully the evolutions of the profiles of dissipation rate and temperature during the diurnal cycle for the first time for

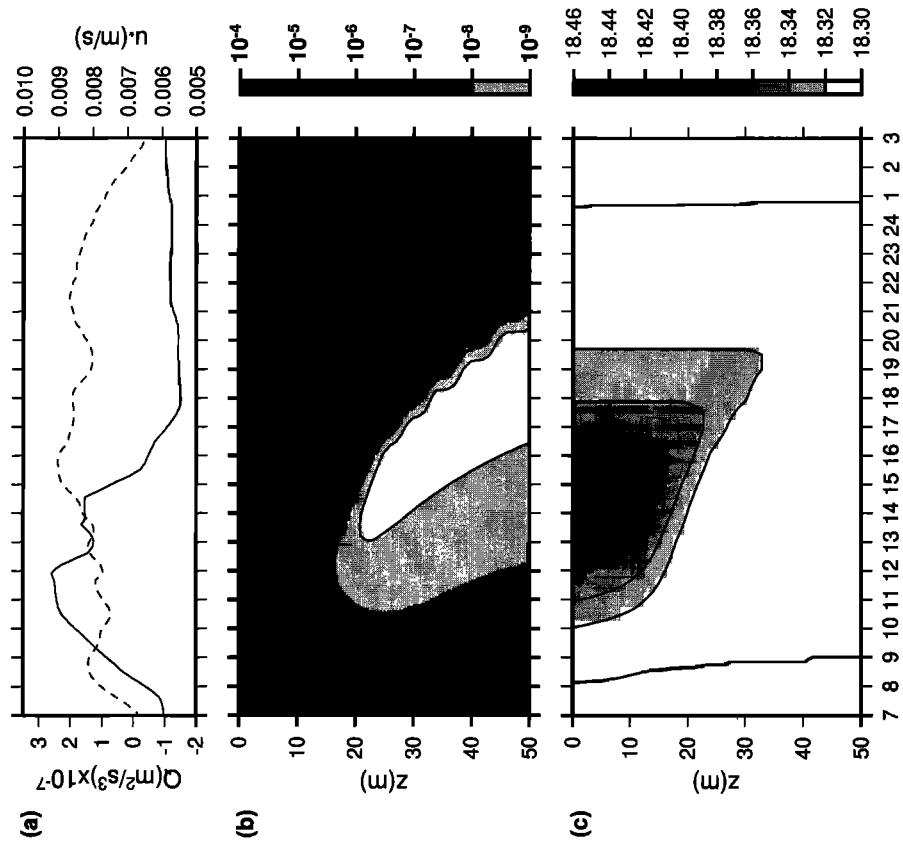

Figure 12. Evolution of the oceanic boundary layer from the simulation (October 18): (a) surface buoyancy flux (solid line) and friction velocity (dashed line), (b) dissipation rate ($m^2\ s^{-3}$), and (c) temperature (°C).

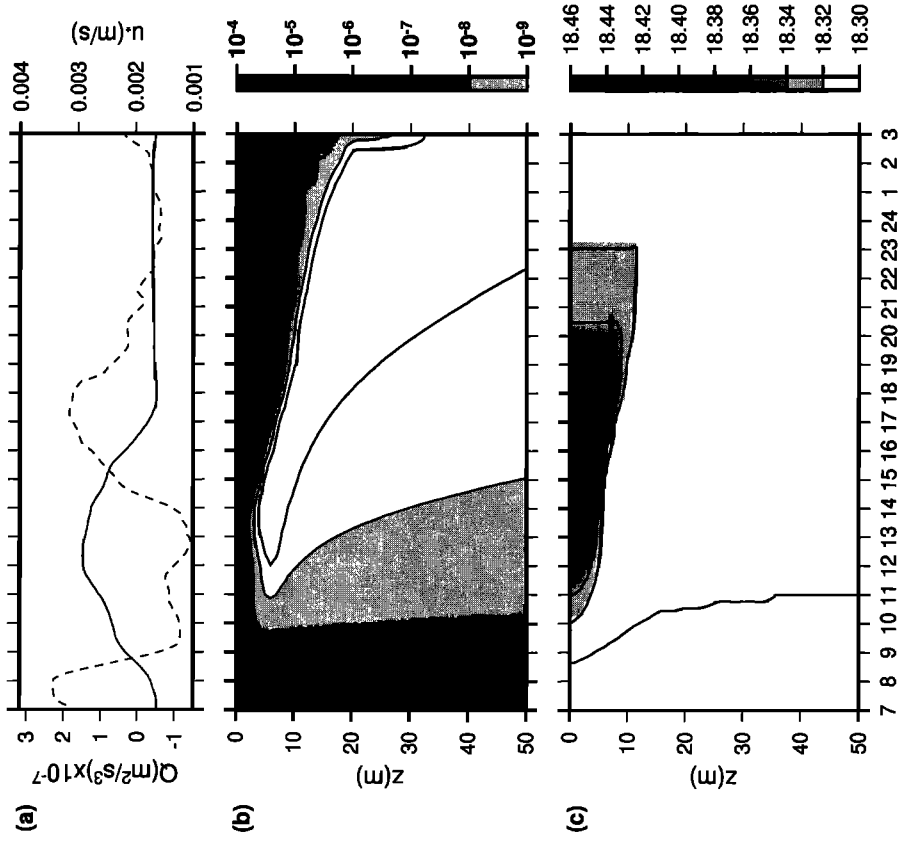

Figure 11. Evolution of the oceanic boundary layer from the simulation (October 13): (a) surface buoyancy flux (solid line) and friction velocity (dashed line), (b) dissipation rate ($m^2\ s^{-3}$), and (c) temperature (°C).

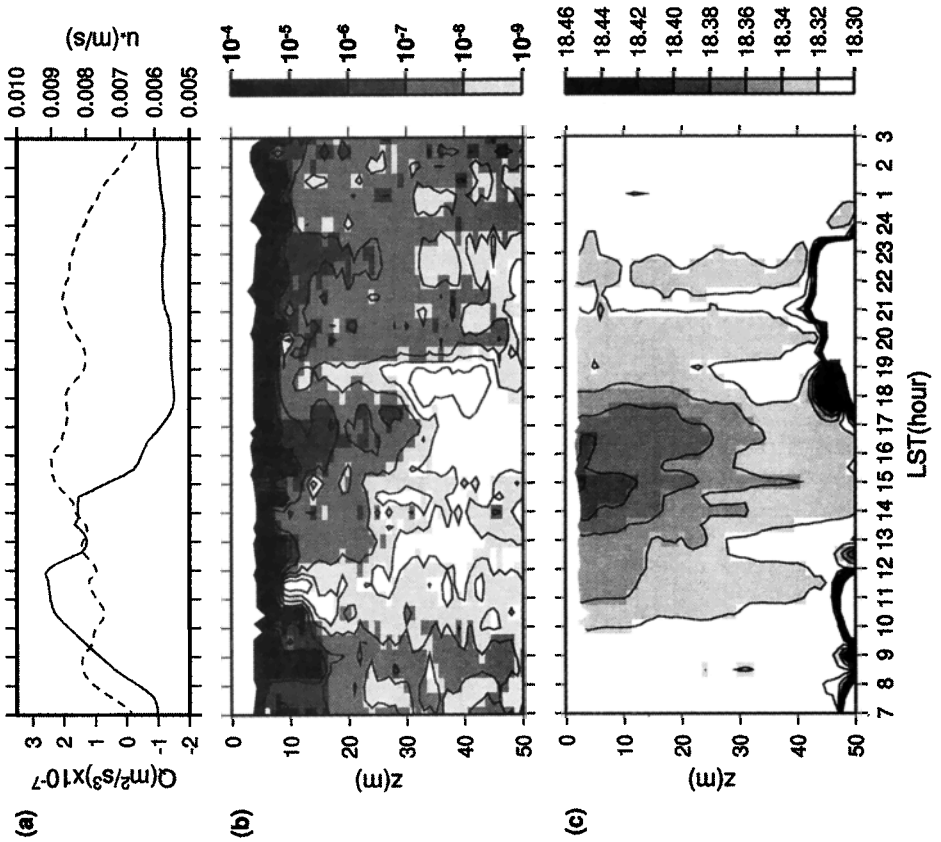

Figure 14. Evolution of the oceanic boundary layer from the observation (October 18): (a) surface buoyancy flux (solid line) and friction velocity (dashed line), (b) dissipation rate ($m^2\ s^{-3}$), and (c) temperature (°C).

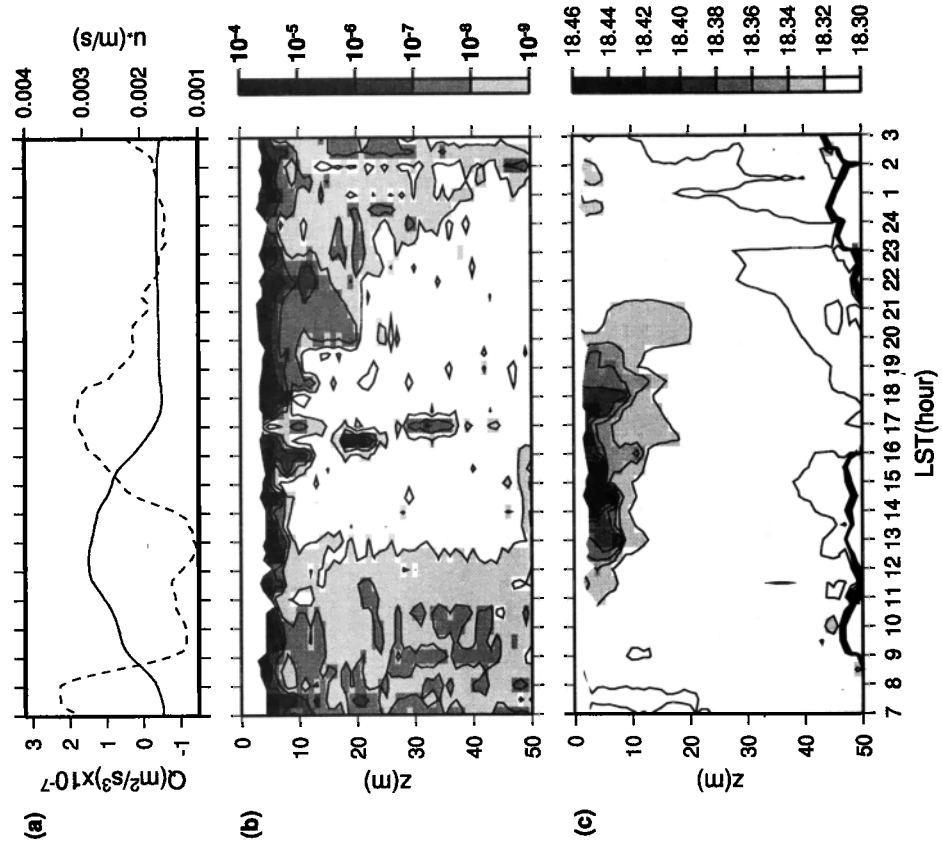

Figure 13. Evolution of the oceanic boundary layer from the observation (October 13): (a) surface buoyancy flux (solid line) and friction velocity (dashed line), (b) dissipation rate ($m^2\ s^{-3}$), and (c) temperature (°C).

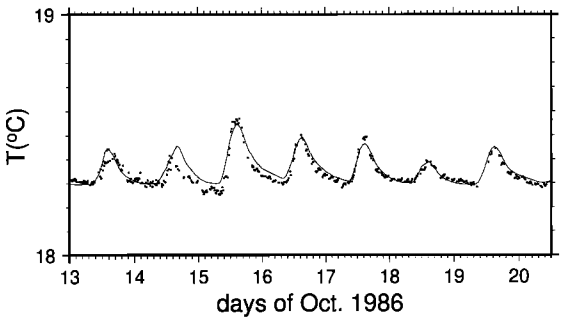

Figure 15. Time series of the observed (dots) and simulated (solid line) sea surface temperature (SST) during PATCHEX.

the case of the observation PATCHEX, as well as the time series of the sea surface temperature over the observation days [*Brainerd and Gregg*, 1993a, b; 1995; *Lombardo and Gregg*, 1989]. The performance of the model was clearly evidenced when compared with the widely used Mellor-Yamada model [*Mellor and Yamada*, 1982]. It was also shown that the model reproduces various typical characteristics of the oceanic boundary layer, for example, the formation of a diurnal thermocline while maintaining a well-mixed layer near the surface under the stabilizing buoyancy flux, the magnitudes of the buoyancy gradients within the mixed layer and at the diurnal thermocline, and the profiles of buoyancy flux and dissipation rate in the convective mixed layer.

Only one empirical constant was adjusted in this model to match the observation data. That is the coefficient α, which represents the stratification effects on turbulence in (17) and (18), and by matching the simulation result with the observation its most appropriate value was found to be $\alpha \approx 120$. It is equivalent to saying that the length scale of eddies is suppressed because of stratification as $l_b \sim 0.09\ q/N$. As to the empirical constants m and z_0, the values suggested by *Craig and Banner* [1994] were used ($m = 100$, $z_0 = 1$ m), and they result in reasonable agreement with the observation data as shown in Figure 9. Given the enormous uncertainty of the near-surface process, both in measurements and theory, further elaboration of the values m and z_0 is extremely difficult at this point. For example, it has been suggested that the TKE flux at the surface depends not only on the frictional velocity but also on the phase velocity of surface waves [*Melville*, 1994; *Gemmrich et al.*, 1994; *Craig*, 1996; *Terray et al.*, 1996].

It should be also mentioned that further improvement of the model is still required since many aspects of the oceanic boundary layer are not clearly represented yet in the present model. For example, the effects of Langmiur circulation and internal wave breaking are not parameterized explicitly yet, although we hope that they may be incorporated implicitly to a certain extent by means of the increased length scale near the surface (equation (14)) and by the parameterization of the eddy viscosity (equation (17)), which allows TKE below the mixed layer, respectively. A more sophisticated scheme is also required in the convective process. Improvement may be acquired by utilizing the results of large eddy simulations of the oceanic boundary layer [*Skyllingstad and Denbo*, 1995; *McWilliams et al.*, 1997] as well as by performing more accurate observations of the oceanic boundary layer.

Finally, the model has been verified only for the diurnal variation of the oceanic boundary layer under a rather normal atmospheric condition in the present paper. For the general application of the model, however, it is important to examine the model for various other cases, including the seasonal variation of the oceanic boundary layer and the response to severe weather conditions.

Acknowledgments. We gratefully thank M. C. Gregg for providing the PATCHEX data. We are also grateful to T. Awaji and T. Yamagata for their interest and comments. This work was supported by the Ministry of Environment (G7 Project), the Ministry of Education of Korea (BSRI-97-5414), KOSEF (Center for Ocean Circulation & Cycles), and Cray Inc. (University R & D Program).

References

Agrawal, Y. C., E. A. Terray, M. A. Donelan, P. A. Hwang, A. J. Williams III, W. M. Drennan, K. K. Kahma, and S. A. Kitaigorodskii, Enhanced dissipation of kinetic energy beneath surface waves, *Nature*, *359*, 219–220, 1992.

Andre, J. C., and P. Lacarrere, Mean and turbulent structure of the oceanic surface layer as determined from one-dimensional third-order simulations, *J. Phys. Oceanogr.*, *15*, 121–132, 1985.

Anis, A., and J. N. Moum, The superadiabatic surface layer of the ocean during convection, *J. Phys. Oceanogr.*, *22*, 1221–1227, 1992.

Anis, A., and J. N. Moum, Prescriptions for heat flux and entrainment rates in the upper ocean during convection, *J. Phys. Oceanogr.*, *24*, 2142–2155, 1994.

Anis, A., and J. N. Moum, Surface wave-turbulence interaction: Scaling $\varepsilon(z)$ near the sea surface, *J. Phys. Oceanogr.*, *25*, 2025–2045, 1995.

Benilov, A. Y., Generation of ocean turbulence by surface waves, *Izv. Russ. Acad. Sci. Atmos. Oceanic Phys.*, *9*, 293–303, 1973.

Blackadar, A. K., The vertical distribution of wind and turbulent exchange in neutral atmosphere, *J. Geophys. Res.*, *67*, 3095–3102, 1962.

Brainerd, K. E., and M. C. Gregg, Diurnal restratification and turbulence in the oceanic surface mixed layer, 1, Observation, *J. Geophys. Res.*, *98*, 22,645–22,656, 1993a.

Brainerd, K. E., and M. C. Gregg, Diurnal restratification and turbulence in the oceanic surface mixed layer, 2, Modeling, *J. Geophys. Res.*, *98*, 22,657–22,664, 1993b.

Brainerd, K. E., and M. C. Gregg, Surface mixed and mixing layer depths, *Deep Sea Res., Part I*, *42*, 1521–1543, 1995.

Britter, R. E., J. C. R. Hunt, G. L. Marsh, and W. H. Snyder, The effects of stable stratification on turbulent diffusion and the decay of grid turbulence, *J. Fluid Mech.*, *127*, 27–44, 1983.

Cane, M. A., Near-surface mixing and the ocean's role in climate, in *Large Eddy Simulation of Complex Engineering and Geophysical Flows*, edited by B. Galperin and S. Orszag, pp. 489–509, Cambridge Univ. Press, New York, 1993.

Craig, P. D., Velocity profiles and surface roughness under breaking waves, *J. Geophys. Res.*, *101*, 1265–1277, 1996.

Craig, P. D., and M. L. Banner, Modeling wave-enhanced turbulence in the ocean surface layer, *J. Phys. Oceanogr.*, *24*, 2546–2559, 1994.

Csanady, G. T., Turbulent diffusion in a stratified fluid, *J. Atmos. Sci.*, *21*, 439–447, 1964.

Davies, A. M., and J. E. Jones, Modeling turbulence in shallow sea regions, in *Small-Scale Turbulence and Mixing in the Ocean*, edited by J. C. J. Nihoul and B. M. Jamart, pp. 63–76, Elsevier, New York, 1988.

Drennan, W. M., M. A. Donelan, E. A. Terray, and K. B. Katsaros, Oceanic turbulence dissipation measurements in SWADE, *J. Phys. Oceanogr.*, *26*, 808–815, 1996.

Garrett, C., Processes in the surface mixed layer of the ocean, *Dyn. Atmos. Oceans*, *23*, 19–34, 1996.

Garwood, R. W., An oceanic mixed layer model capable of simulating cyclic states, *J. Phys. Oceanogr.*, *7*, 455–468, 1977.

Gaspar, P., Modeling the seasonal cycle of the upper ocean, *J. Phys. Oceanogr.*, *18*, 161–180, 1988.

Gemmrich, J. R., T. D. Mudge, and V. D. Polonichko, On the energy input from wind to surface waves, *J. Phys. Oceanogr.*, *24*, 2413–2417, 1994.

Hopfinger, E. J., Turbulence in stratified fluids: A review, *J. Geophys. Res.*, *92*, 5287–5303, 1987.

Hopfinger, E. J., and J. A. Toly, Spatially decaying turbulence and its relation to mixing across density interface, *J. Fluid Mech.*, *78*, 155–175, 1976.

Kantha, L. H., and C. A. Clayson, An improved mixed layer model for geophysical application, *J. Geophys. Res.*, *99*, 25,235–25,266, 1994.

Kitaigorodskii, S. A., *The Physics of Air-Sea Interaction*, 237 pp., Isr. Program for Sci. Transl., Jerusalem, 1970.

Kitaigorodskii, S. A., and J. L. Lumley, Wave-turbulence interactions in the upper ocean, I, The energy balance of the interacting fields of surface wind waves and wind-induced three-dimensional turbulence, *J. Phys. Oceanogr.*, *13*, 1977–1987, 1983.

Kitaigorodskii, S. A., and Y. Z. Miropolskii, Turbulent-energy dissipation in the ocean surface layer, *Izv. Russ. Acad. Sci. Atmos. Oceanic Phys.*, *4*, 647–659, 1968.

Klein, P., and M. Coantic, A numerical study of turbulent process in the marine upper layers, *J. Phys. Oceanogr.*, *11*, 849–863, 1981.

Kraus, E. B., Merits and defects of different approaches to mixed layer modelling, in *Small-Scale Turbulence and Mixing in the Ocean*, edited by J. C. J. Nihoul and B. M. Jamart, pp. 37–50, Elsevier, New York, 1988.

Kraus, E. B., and J. S. Turner, A one-dimensional model of the seasonal thermocline, *Tellus*, *19*, 98–106, 1967.

Large, W. G., J. C. McWilliams, and S. C. Doney, Oceanic vertical mixing: A review and a model with a nonlocal boundary layer parameterization, *Rev. Geophys.*, *32*, 363–403, 1994.

Lombardo, C. P., and M. C. Gregg, Similarity scaling of viscous and thermal dissipation in a convecting surface boundary layer, *J. Geophys. Res.*, *94*, 6273–6284, 1989.

Martin, P. J., Simulation of the mixed layer at OWS November and Papa with several models, *J. Geophys. Res.*, *90*, 903–916, 1985.

McWilliams, J. C., P. P. Sullivan, and C. H. Moeng, Langmuir turbulence in the ocean, *J. Fluid Mech.*, *334*, 1–30, 1997.

Mellor, G. L., and P. A. Durbin, The structure and dynamics of the ocean surface mixed layer, *J. Phys. Oceanogr.*, *5*, 718–728, 1975.

Mellor, G. L., and T. Yamada, Development of a turbulent closure model for geophysical fluid problems, *Rev. Geophys.*, *20*, 851–875, 1982.

Melville, K. W., Energy dissipation by breaking waves, *J. Phys. Oceanogr.*, *24*, 2041–2049, 1994.

Niiler, P. P., and E. B. Kraus, One dimensional models of the upper ocean, in *Modeling and Prediction of the Upper Layers of the Ocean*, edited by E. B. Kraus, pp. 143–172, Pergamon, Tarrytown, N.Y., 1977.

Noh, Y., Dynamics of diurnal thermocline formation in the oceanic mixed layer, *J. Phys. Oceanogr.*, *26*, 2183–2195, 1996.

Noh, Y., and H. J. S. Fernando, A numerical study on the formation of a thermocline in shear-free turbulence, *Phys. Fluids A*, *3*, 422–426, 1991.

Osborn, T., D. M. Farmer, S. Vagle, S. A. Thorpe, and M. Cure, Measurements of bubble plumes and turbulence from a submarine, *Atmos. Ocean*, *30*, 419–440, 1992.

Paulson, C. A., and J. J. Simpson, Irradiance measurements in the upper ocean, *J. Phys. Oceanogr.*, *7*, 952–956, 1977.

Phillips, O. M., *The Dynamics of the Upper Ocean*, Cambridge Univ. Press, New York, 1977.

Phillips, O. M., Spectral and statistical properties of the equilibrium range of wind-generated gravity waves, *J. Fluid Mech.*, *156*, 171–185, 1985.

Price, J. F., R. A. Weller, and R. Pinkel, Diurnal cycling: Observations and models of the upper ocean response to diurnal heating, cooling and wind mixing, *J. Geophys. Res.*, *91*, 8411–8427, 1986.

Rosati, A., and K. Miyakoda, A general model for upper ocean simulation, *J. Phys. Oceanogr.*, *18*, 1601–1626, 1988.

Shay, T. J., and M. C. Gregg, Convectively driven turbulent mixing in the upper ocean, *J. Phys. Oceanogr.*, *16*, 1777–1798, 1986.

Skyllingstad, E. D., and D. W. Denbo, An ocean large-eddy simulation of Langmuir circulations and convection in the surface mixed layer, *J. Geophys. Res.*, *100*, 9501–8522, 1995.

Stillinger, D. C., K. N. Helland, and C. W. van Atta, Experiments on the stratification of homogeneous turbulence to internal waves in a stratified fluid, *J. Fluid Mech.*, *131*, 91–122, 1983.

Stull, R. B., *An Introduction to Boundary Layer Meteorology*, Kluwer Acad., Norwell, Mass., 1988.

Terray, E. A., M. A. Donelan, Y. C. Agrawal, W. M. Drennan, K. K. Kahma, A. J. Williams III, P. A. Hwang, and S. A. Kitaigorodskii, Estimates of kinetic energy dissipation under breaking waves, *J. Phys. Oceanogr.*, *26*, 792–807, 1996.

Thompson, S. M., and J. S. Turner, Mixing across an interface due to turbulence generated by an oscillating grid, *J. Fluid Mech.*, *67*, 349–368, 1975.

Thorpe, S. A., Bubble clouds and the dynamics of the upper ocean, *Q. J. R. Meteorol. Soc.*, *118*, 1–22, 1992.

Toba, Y., and H. Kawamura, Wind-wave coupled downward-Bursting boundary layer (DBBL) beneath the sea surface, *J. Oceanogr.*, *52*, 409–419, 1996.

Wyngaard, J. C., Structure of the planetary boundary layer and implications for its modeling, *J. Clim. Appl. Meteorol.*, *24*, 1131–1142, 1985.

Yu, L., and J. J. O'Brien, Variational estimation of the wind stress drag coefficient and the oceanic eddy viscosity profile, *J. Phys. Oceanogr.*, *21*, 709–718, 1991.

H. J. Kim and Y. Noh, Department of Atmospheric Sciences, Yonsei University, Seoul 120-749, Korea. (noh@atmos.yonsei.ac.kr)

(Received December 8, 1997; revised November 13, 1998; accepted March 4, 1999.)